Nanoscale enzymatic compartments in tandem support cascade reactions in vitro

SCHOLARONE™
Manuscripts

Nanoscale enzymatic compartments in tandem support cascade reactions *in vitro*

Andrea Belluati[1], Ioana Craciun[1], Juan Liu[1], Cornelia G. Palivan[1] *

[1]Department of Chemistry, University of Basel, Mattenstrasse 24a, CH-4058 Basel

KEYWORDS

Catalytic compartment, polymersome, cascade reaction, *in vitro*, gout

ABSTRACT

Compartmentalization at the nanoscale is fundamental in nature, where the spatial segregation of biochemical reactions within cells ensures optimal conditions for regulating metabolic pathways. Here, we present a nature inspired approach to engineer enzymatic cascade reactions taking place between separate vesicular nanocompartments (polymersomes), each containing one enzyme type. We propose by the selected combination of enzymes, an efficient solution to detoxify the harmful effect of uric acid and prevent the accumulation of the derived H_2O_2, both being associated with various pathological conditions (e.g. gout and oxidative stress). Fungal uricase and horseradish peroxidase combined to act in tandem, were separately encapsulated within nanocompartments, equipped with channel porins as gates to allow passage of substrates and products from each step of the reaction. We established the molecular factors affecting the efficiency of the overall reaction, and the protective role of the compartments. Interestingly, the

21 cascade reaction between separate nanocompartments was as efficient as for free enzymes in

22 complex media, such as human serum. The nanocompartments were non-toxic towards cells and

23 more importantly, addition of the tandem catalytic nanocompartments to cells exposed to uric

24 acid provided simultaneous detoxification of uric acid and the H_2O_2. Such catalytic

25 nanocompartments can be used as a platform for understanding fundamental factors affecting

26 intra-cellular communication and introduce non-native metabolic reactions into living systems

27 for therapeutic applications.

28

Introduction

29

30 In nature, various enzymatic reactions occur in confined environments where substrates are

31 channeled in between enzymes, or signaling molecules are released and travel between

32 compartments[1] serving to isolate reactive intermediates, concentrate substrates in a specific

33 region or fine tune reaction pathways.[2] Inspired by nature, significant efforts have been made to

34 confine enzymes within nanocompartments, such as protein cages, lipid/polymer based

35 compartments and layer by layer capsules, resulting in enzymatic compartments.[1, 3-4] Enzymatic

36 compartments are of particular interest as they offer a protective environment that increases the

37 life-time of the encapsulated enzymes, essential for applications.[5-6] In this respect, a particularly

38 appealing class of compartments are polymersomes generated by self-assembly of amphiphilic

39 copolymers, as their membrane is more stable than the lipid membrane of liposomes, while

40 maintaining biocompatibility if the chemical nature of the copolymer is appropriately selected.[7]

41 A key aspect to allow the enzymatic reaction to take place *in situ,* inside the cavity of

42 polymersomes, is to render their membrane permeable thus enabling an exchange of substrates

43   and products with their surroundings. Various approaches have been reported: i) using inherently

44   porous polymersomes,[8-9] ii) using an external stimulus, such as pH, or by addition of a chemical

45   agent to render the membrane permeable,[10-11] and iii) inserting biopores or membrane proteins in

46   the membrane.[12-13]

47   Cascade reactions reported within nanocompartments mainly involve encapsulation of one type

48   of enzyme and providing the second enzyme free in the surrounding medium.[6, 14] However, if

49   one partner of the cascade reaction is free in solution it might be degraded, resulting in a

50   decrease or even termination of the overall reaction. Co-encapsulating enzymes within the same

51   nanocompartment solves this issue, but only a low co-encapsulation efficiency can be obtained

52   due to the statistic process of formation of multi-enzyme-loaded polymersomes.[7]

53   A higher encapsulation efficiency of different enzymes can be achieved by linking the two

54   enzymes together prior to encapsulation, using micrometer-sized compartments or the formation

55   of compartments within compartments where small compartments and free enzymes are

56   encapsulated inside micrometer-size compartments.[9, 15-18] Both binding the enzymes in one

57   complex and the approach of compartments within compartments, which uses organic solvents

58   and emulsions, have the disadvantage of hindering the catalytic activity of the enzymes thus

59   decreasing the efficiency or blocking the reaction.

60   One approach, which allows for modularity while preserving the enzymes involved in the

61   cascade reaction, is to design catalytic compartments working in tandem.[7] However, there are

62   only very few examples of catalytic nanocompartments (CNCs) working in tandem[8, 10, 19-20] and,

63   to the best of our knowledge, very few polymeric nanocompartments were evaluated in a more

64   complex medium or *in vitro*.[21] In addition, the kinetics of the cascade reactions in separate

65   compartments and the molecular factors affecting them were not investigated to determine

66 whether such CNCs still function in a more complex medium than buffers or to propose a

67 therapeutically relevant solution.

68 Here, we present a bio-inspired approach to engineer CNCs working in tandem and propose, by

69 an appropriate selection of the enzymes, an efficient solution to detoxify the harmful effect of

70 uric acid and H_2O_2, associated with various pathologic conditions (e.g. gout and oxidative

71 stress). Both gout and oxidative stress are known to induce severe health problems, associated

72 with an increase in medical costs estimated to be above \$6 billion per year in the US.[22] We used

73 an amphiphilic block copolymer poly(2-methyloxazoline)-*block*-poly(dimethylsiloxane)-*block*-

74 poly(2-methyloxazoline)   ($PMOXA_6$-$PDMS_{44}$-$PMOXA_6$)   for   the   formation   of   the

75 nanocompartments,[23] and their membrane was rendered permeable by insertion of the bacterial

76 porin Outer membrane protein F (OmpF).[24] The role of the polymersomes is to protect the

77 encapsulated enzymes in order to prolong their stability, as a crucial step towards translational

78 applications, as is intended by our selected enzymatic reaction. We selected as enzymes for the

79 cascade reaction uricase (UOX) and horseradish peroxidase (HRP), which uses H_2O_2 produced

80 by UOX, as the substrate to initiate the second reaction (Scheme 1).[25-27] This non-native

81 combination of enzymes serves to sequentially decrease the concentration of uric acid and

82 prevent the accumulation of H_2O_2, derived from the reaction of uric acid degradation, thus

83 resulting in a dual therapeutic approach. While previous reports on cascade reactions between

84 nanocompartments focused on the feasibility of model reactions,[20] here we go one step further to

85 understand the molecular factors associated with the cascade reaction between separate

86 compartments and to optimize their overall function. Next, we investigate their ability to

87 function at increasing distances to mimic intra- and intercellular bio-distances as well as in

88 human serum, prior to applying them to decrease uric acid and the accumulation of H_2O_2, from

89   the cellular milieu to advance their therapeutic application. Our approach opens the avenue to

90   combine different enzymes inside separate nanocompartments to obtain complex, novel-to-

91   nature enzymatic pathways with high potential in diagnostics and therapeutics.

92
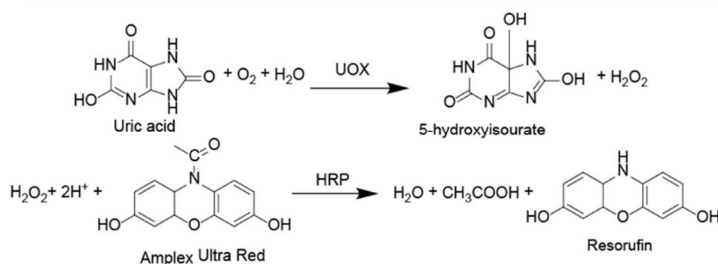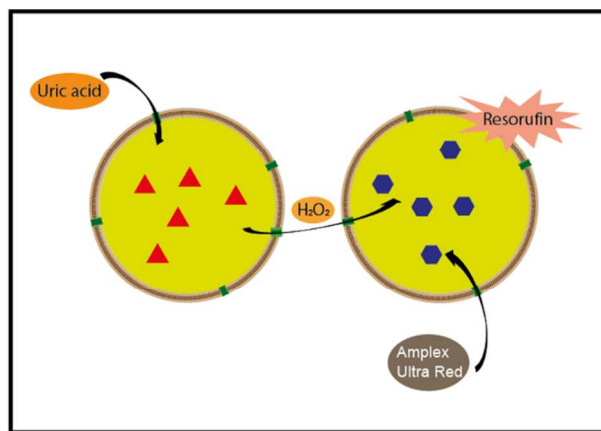
Scheme 1. *Schematic representation of catalytic nanocompartments (OmpF: green rectangle) working in tandem and detailed*

94   *cascade reaction mediated by a combination of uricase (UOX, red triangles) and horseradish peroxidase (HRP, blue hexagons).*

95   *The oxidation of uric acid results in formation of 5-hydroxyisourate and hydrogen peroxide. The latter is a co-substrate for HRP*

96   *in presence of substrate Amplex Ultra Red, AR. The final product, resorufin, can be monitored by fluorescence spectroscopy.*

97

Materials

99   Dulbecco's Modified Eagle Medium with 4.5 g L^{-1} D-Glucose (DMEM-GlutaMax) was

100   purchased from Gibco life technologies. Fetal calf serum (FCS) was purchased from

101   BioConcept. CellTiter 96® Aqueous One Solution Cell Proliferation Assay (MTS) was

102   purchased from Promega. The triblock copolymer $PMOXA_6$-$PDMS_{44}$-$PMOXA_6$ was kindly

5

103   provided by Prof. W. Meier, the University of Basel.[23] All other reagents and enzymes were

104   purchased from Sigma-Aldrich unless otherwise specified.

Methods

OmpF expression and extraction

107   Wild-type OmpF was obtained according to a previously reported protocol,[28] with a few

108   modifications: bacteria was grown at 30 °C for 6 hours on Terrific Broth (TB) (Difco, USA) and

109   all ultracentrifugations were performed at room temperature (RT).

Preparation of catalytic nanocompartments

111   All CNCs were prepared at RT using the triblock copolymer $PMOXA_6$-$PDMS_{44}$-$PMOXA_6$

112   (obtained according to a previously reported procedure[23]) and wild-type OmpF, via the film

113   rehydration technique. Films were rehydrated to a final polymer concentration of 4 mg mL^{-1} with

114   0.25 mg of UOX or HRP in PBS (pH 7) and 50 μl of previously dialyzed OmpF (60 μg mL^{-1}

115   final concentration) or an equivalent volume of dialyzed octyl glucopyranoside, OG (Anatrace,

116   USA) 3% for the non-permeabilized CNCs. Samples were extruded through an Avanti mini-

117   extruder (Avanti Polar Lipids, USA) with a 200 nm pore diameter polycarbonate membrane (11

118   times). Non-encapsulated enzyme was removed through size exclusion chromatography (SEC)

119   (Sepharose 4B column; 30 cm length).

120

Catalytic nanocompartment characterization — Static and Dynamic light scattering

122   Light scattering (LS) experiments were performed at 25 °C, using an ALV/CGS–8F goniometer

123   (Langen/Hessen, Germany) equipped with a frequency-doubled He-Ne laser (LS instruments, λ

124   = 633). Static light scattering (SLS) was performed in 5° steps between 50° and 135° and

125   analyzed with Zimm plot software (LS Instruments). Dynamic light scattering (DLS) was

126   performed at 90° and analyzed through nonlinear decay-time analysis supported by cumulant fit.

127

128   *Catalytic nanocompartment characterization — Transmission electron microscopy (TEM)*

129   CNC suspensions in PBS at 0.25 mg mL^{-1} were deposited on glow-discharged carbon grids

130   (Quantifoil, Germany) stained with 1.5% uranyl acetate solution and deposited on carbon-coated

131   copper grids. A transmission electron microscope (Philips Morgagni 268D) at 293 K was used.

132

133   *Catalytic nanocompartment characterization — Fluorescence correlation spectroscopy*

134   Vesicles were labeled with BODIPY 630/650 SE (Thermo Fisher Scientific, USA) 100 nM.

135   All measurements were carried out using an LSM 880 confocal laser microscope (Carl Zeiss,

136   Germany) with a 40x, 1.2 water immersion C-Apochromat objective lens. Measurements were

137   performed at RT using a sample volume of 20 μL on a 22x50 mm glass slide. A HeNe laser at

138   633 nm was used for excitation of the BODIPY fluorophore, at 1% attenuation and pinhole 62

139   μm. The fluorescence signal was measured in real time and the autocorrelation function was

140   calculated by the software calculator QuickFit 3.0.[29] Measurements were recorded over 5 s and

141   each measurement was repeated 30 times. Experimental auto correlation curves were fitted using

142   a two-component model including triplet state:

$$G(\tau) = 1 + \left(1 + \frac{T}{1-T} e^{-\frac{\tau}{\tau_{trip}}}\right) \frac{1}{N} \left(\frac{f_1}{1 + \frac{\tau}{\tau_{D1}} \sqrt{1 + R^2 \frac{\tau}{\tau_{D1}}}} + \frac{f_2}{1 + \frac{\tau}{\tau_{D2}} \sqrt{1 + R^2 \frac{\tau}{\tau_{D2}}}} \right)$$

143   f_1 and f_2 are respectively the fraction of the particles of the corresponding component 1 (dye) or 2

144   (vesicles), τ_{D1} represents the diffusion time of the dye and τ_{D2} the diffusion time of the vesicles, T

145   the fraction of fluorophores in triplet state with triplet time τ_{trip}, N is the number of particles and

146   R the structural parameter, fixed at 5, according to the guidelines from Zeiss. The τ_{trip} and τ_D of

147   free dye were determined independently, and subsequently fixed in the fitting procedure for dye-

148   interacting vesicles. The confocal volume of 1 fL, was obtained by a calibration with free

149   BODIPY and was necessary to determine the concentration of fluorescent particles (knowing the

150   number of particles detected in the volume).

151

Enzyme quantification

153   The non-encapsulated enzyme fraction was recovered via SEC and the enhanced Pierce™

154   Bicinchonic Acid (BCA) assay was performed according to the supplier's protocol (Thermo

155   Fisher Scientific, USA); instead of the BSA standards, both UOX (35 U mg^{-1}) and HRP (300 U

156   mg^{-1}) calibration curves were prepared for the quantification of the respective samples. The

157   amount of un-encapsulated protein was multiplied by the volume recovered from the column and

158   then subtracted from the amount initially added to the rehydration solution, yielding the total

159   amount of enzymes within the vesicles, divided by the volume of the vesicle (first fraction), *i.e.*

160   the final concentration of the protein. This was performed on samples with no inserted OmpF,

161   because the presence of the hydrophobic porin is not expected to influence the encapsulation

162   efficiency of hydrophilic enzymes. The number of enzyme molecules was then divided by the

163   number of vesicles, obtaining the number of enzymes per vesicle.

164

Enzyme activity and kinetics

166   Kinetic parameters were calculated using the Michaelis-Menten model:

$$v = \frac{V_{max}[S]_0}{K_M + [S]_0}$$

$$k_{cat} = \frac{V_{max}}{[E]_0}$$

167   Where v is the velocity of the enzyme, V_{max} is the maximum velocity at saturating concentration,

168    $[S]_0$ is initial the concentration of the substrate S, K_M is the Michaelis-Menten constant. k_{cat} is the

169   turnover number, the number of chemical conversions per second, $[E]_0$ is the concentration of

170   catalytic sites (both for UOX and HRP it is equivalent with the concentration of enzyme).

171   In all experiments involving a cascade reaction, UOX was added in excess to HRP, to partially

172   compensate for the former enzyme's lower activity, so that the ratio between production (from

173   UOX, 35 U mg^{-1}) and consumption (from HRP, 350 U mg^{-1}) of hydrogen peroxide would not be

174   the limiting factor. All enzymatic measurements were performed using a Spectramax M5

175   microplate reader (Molecular Devices, USA), in a in a 96-well, flat bottomed UV-transparent

176   plate (Corning, USA) for uric acid absorbance (290 nm) or in a black plate (Thermo Fisher

177   Scientific) for resorufin fluorescence (excitation 570 nm / emission 595 nm). The final volume in

178   each well was of 200 µL in PBS. UOX concentration was increased ten-fold in cascade reaction

179   experiments, to counter the slower native activity per weight of the enzyme, compared to the

180   downstream enzyme HRP. Both uric acid consumption and resorufin production were quantified

181   by means of calibration curves ($R^2 > 0.9$ for both curves). Each experiment was performed in

182   triplicate and data was collected over 15 minutes (10 for the measurement of kinetic parameters).

183

184   *UOX kinetics*

185   UOX or UOX-loaded CNCs (final concentration of 3 µg mL^{-1}) were incubated in presence of

186   increasing concentrations of the substrate uric acid (25, 100, 200, 400 and 800 µM) and the

187   initial velocity of the enzymatic reaction was determined. The consumption of uric acid was

188 monitored and the data fitted with Graphpad Prism 7 software, obtaining K_M, V_{max} and k_{cat}

189 values.

190

HRP kinetics

192 HRP or HRP-loaded CNCs (final concentration of 3 µg mL^{-1}) were incubated in the presence of

193 10 µM H_2O_2 and increasing concentrations of Amplex Ultra Red (AR) (Invitrogen) ranging from

194 0.2 to 20 µM. The initial velocity of the enzymatic reaction was determined by monitoring the

195 formation of resorufin. The data was fitted using Graphpad Prism 7 software, obtaining K_M, V_{max}

196 and k_{cat} values.

197

UOX-HRP cascade kinetics

199 Both reactions were examined when in a cascade: UOX or UOX-loaded CNCs (final

200 concentration of 3 µg mL^{-1}) were added to HRP or HRP-loaded CNCs (final concentration 300

201 ng mL^{-1}) and both uric acid and AR were alternatively varied according to the previously listed

202 concentrations.

203

Amplex Ultra Red conversion assay in a cascade

205 The same cascade reaction was tested at different conditions: UOX or UOX-loaded CNCs (final

206 concentration of 3 µg mL^{-1}) were added to HRP or HRP-loaded CNCs (final concentration 300

207 ng mL^{-1}), uric acid to a final concentration of 10 µM and AR to a final concentration of 1 µM,

208 unless in controls where either substrate was missing and was substituted by the same volume of

209 PBS. The reaction profile in presence of catalase (1000 U mg^{-1}, final concentration of 10 µg mL^{-}

210   [1]) was blanked against the reaction profile of catalase alone in presence of AR, as catalase too

211   has a heme center capable of reacting with the fluorogenic molecule.

212

Catalytic nanocompartment resilience to degrading agents

214   Concentrations were 3 µg mL^{-1} for UOX or UOX-CNC and 300 ng mL^{-1} for HRP or HRP-CNC.

215   For the heat resistance assay, aliquots of the polymersome were incubated at 37, 50, 60 and 75

216   °C for either 10 or 30 minutes. For the chemical and enzymatic resistance assays, aliquots were

217   incubated with 6 M guanidine hydrochloride (GdnHCl) for 1 hour and 0.1 mg ml^{-1} Proteinase K

218   for 2 hours (37 °C), respectively. Proteinase K was added in excess with respect to the other

219   enzymes (free and encapsulated). The production of resorufin was compared to that of the

220   cascade reaction with no additional elements and the ratio was calculated. To verify unspecific

221   binding, the same amount of enzyme (either UOX or HRP) was added to pre-formed empty

222   vesicles and then purified with the same protocol, then mixed with vesicles encapsulating the

223   other enzyme and the cascade kinetics were followed.

224

Activity of CNCs in serum

226   Activity in biological fluid was tested in human blood serum in which uric acid was dissolved to

227   a final concentration of 500 µM at 37 °C, mimicking hyperuricemia. UOX or UOX-CNCs were

228   added to reach a final concentration of 18 µg ml^{-1}, HRP or HRP-CNCs to 900 ng ml^{-1}, AR to 10

229   µM. The decrease of absorbance at 290 nm was monitored over the course of 6 hours. The

230   degradation of uric acid was defined as

231    $$Relative\ urate\ degradation = \frac{\frac{\Delta Abs290_{with\ enzyme}}{min}}{\frac{\Delta Abs290_{no\ enzyme}}{min}},$$

232

233 *Dependence of distance over reaction efficiency*

234 Knowing the amount of CNCs in a given volume (obtained from FCS measurements), it was

235 possible to calculate the mean inter-vesicle distance, assuming a cubic space occupied by the

236 compartments, as

$$\frac{1}{\sqrt[3]{\dfrac{N}{V}}}$$

237 where N is the number of particles (sum of UOX and HRP loaded-polymersomes) and V is the

238 reaction volume. A constant concentration of UOX-CNCs was mixed with a solution of HRP-

239 CNCs at concentrations: 2x, 1x, 0.5x, 0.25x, 0.1x, 0.02x, 0.01x and 0.005x. The decrease in

240 concentration of HRP-CNCs induced an increase of the mean distance between polymersomes,

241 which was calculated using $N = N_{UOX-CNC} + N_{HRP-CNC}$. Resorufin production was monitored as

242 described above.

243

244 *Cell culture*

245 HEK293T cells were cultured in a humidified atmosphere with 5% CO_2 at 37 ^{o}C in Dulbecco's

246 Modified Eagle Medium with GlutaMAX^{TM}-I (4.5 g L^{-1} D-Glucose, Gibco life technologies) and

247 supplemented with 10% Fetal calf serum (FCS, BioConcept), 100 U mL^{-1} penicillin and 100 µg

248 mL^{-1} streptomycin (Sigma Aldrich).

249

250 *Cell viability assay-MTS*

251 For cell viability assessment, a CellTiter 96® Aqueous One Solution Cell Proliferation Assay

252 (MTS, Promega) was used according to manufacturer instructions. Cells were seeded (5 000

253 cells/well in 100 µL cell culture medium) in a 96-well plate and incubated for 24 h. After 24 h

254   the UOX-HRP-CNCs (concentrations ranging from 1.18 to 18 μg mL^{-1} of total polymer) were

255   diluted in PBS and added to the cells to reach a final volume of 200 μ/well. After 24 h incubation

256   in presence of the CNCs, 20 μL MTS reagent was added to each well. After 4 h absorbance was

257   measured at 490 nm using a Spectramax M5e plate reader. Background absorbance from control

258   wells containing all assay components without cells was subtracted from each well and data

259   normalized to control cells containing all components except CNCs.

260

261   *Cell viability in presence of uric acid*

262   Cells were seeded at a density of 5 000 cells/well in 100 μL cell culture medium, in a 96-well

263   plate and incubated for 24 h. Next, cells were dosed with 250 or 500 μM of uric acid, final

264   concentration, in the presence or absence of UOX-HRP-CNCs (18 μg mL^{-1} for UOX and 0.9 μg

265   mL^{-1} for HRP, final concentrations in 200 μL final volume) or in the presence of free enzymes

266   (UOX and HRP) at the same concentration. AR (1 μM, final concentration in 200 μL final

267   volume) was added to each well as a co-substrate for the HRP-CNCs. After a 24 h incubation

268   period, 20 μL MTS reagent was added to each well. The absorbance was measured at 490 nm

269   after 4 h. Background absorbance from control wells containing all assay components apart from

270   the cells was subtracted from each well and data normalized to control cells containing all

271   components except CNCs and uric acid.

272

273   *Statistics*

274   Multiple t-tests were performed using Graphpad Prism 7 software, comparing datasets, without

275   assuming constant standard deviation (SD). Statistical significance ($p < 0.05$) was corrected using

276   the Holm-Sidak method. Significance was marked as * $p < 0.05$, ** $p < 0.01$, *** $p < 0.001$,

277   sample size was always n = 3.

278

Results and Discussion

279

Formation of UOX-Catalytic nanocompartments and HRP-Catalytic nanocompartments

280

281   We encapsulated UOX and HRP inside the supramolecular assemblies formed during the self-

282   assembly process of the copolymer by using film rehydration method due to its mild conditions,

283   which do not affect the biomolecules.[7, 30] The architecture of the supramolecular assemblies in

284   presence and absence of enzymes was established by a combination of LS and TEM. We used

285   SLS to obtain the radius of gyration R_g, and DLS for the hydrodynamic radius R_h. The ratio of

286   these values R_g/R_h, called ρ-factor, is indicative of the different architectures, e.g. 1 for hollow

287   spheres while 0.77 for solid spheres.[31] In the case of empty supramolecular assemblies, R_g and

288   R_h values were 70 ± 33 nm and 84 ± 25 nm respectively, and the calculated ρ-factor of 0.96

289   indicates hollow sphere architecture, thus formation of polymersomes. In the presence of UOX

290   (UOX-CNC), we determined for the supramolecular assemblies an R_g of 68 ± 12 nm and R_h of

291   73 ± 33 nm (ρ = 0.95), while in the presence of HRP (HRP-CNC) they had an R_g of 74 ± 35 nm

292   and R_h 85 ± 41 nm (ρ = 0.87) (Figure S1). In both cases, the enzymes did not affect the self-

293   assembly process and resulted in polymersome architecture, which agrees with the TEM

294   micrographs (Figure 1A and 1C, Figure S2 and S3).

295   In order to quantify the amount of encapsulated enzymes inside the nanocompartments, we used

296   a combination of brightness measurements in FCS and BCA. FCS measures the fluorescence

297   fluctuations due to the Brownian motion of fluorescent species in a fL-sized volume, yielding

298   molecular parameters such as diffusion time and the number of particles that can be used to

299 evaluate interactions/encapsulation of the fluorescent dyes with/in supramolecular assemblies.[32]

300 By labeling the vesicle membrane with BODIPY 630/650, and using a 2-component fit (fixing

301 the diffusion time of free dye as one of the components) we obtained their average diffusion time

302 (τ_D 5000 μs for both CNCs, as compared to τ_D = 57 μs of the free dye) and overall number of

303 fluorescent vesicles in solution. The fraction of dye-polymersomes was 99% for UOX-CNCs and

304 94% for HRP-CNCs (2.6×10^{11} and 3.9×10^{11} polymersomes μL^{-1}, respectively), while that of the

305 free dye 1% and 4% thus indicating that most of the dye partitioned into the polymersome

306 membrane (Figure 1B and 1D).

307 A total protein concentration of 30 μg mL^{-1} for UOX and 18.6 μg mL^{-1} for HRP, was obtained

308 by BCA assay (Figure S4). Dividing the protein concentration by the number of polymersomes

309 obtained by brightness measurements, we determined an average of 11 ± 7 enzymes in UOX-

310 CNCs and 6 ± 2 enzymes in HRP-CNCs. An encapsulation efficiency of 36 ± 12 % for UOX and

311 $22 \pm 4\%$ for HRP inside CNCs was obtained, in agreement with the encapsulation efficiency

312 values obtained for other enzymes inside polymersomes.[7, 30] A number of 11

313 OmpF/polymersome was inserted as we used similar conditions as previously reported.[33] We

314 kept the amount of porin constant in order to distinguish the effect of all other molecular factors
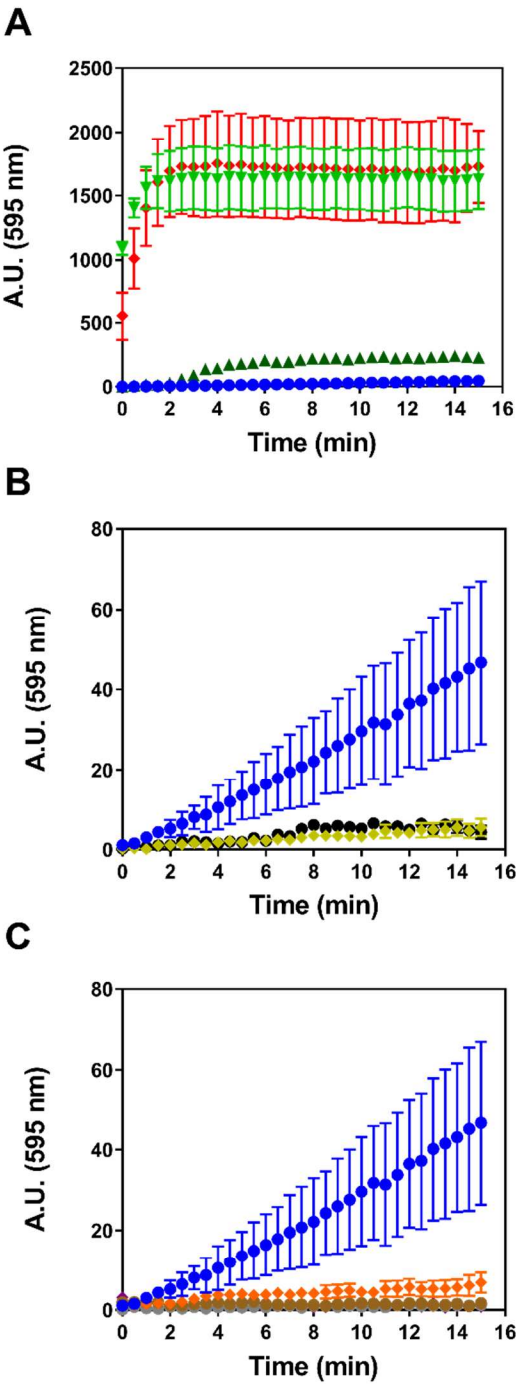
315 on the cascade reaction.

316
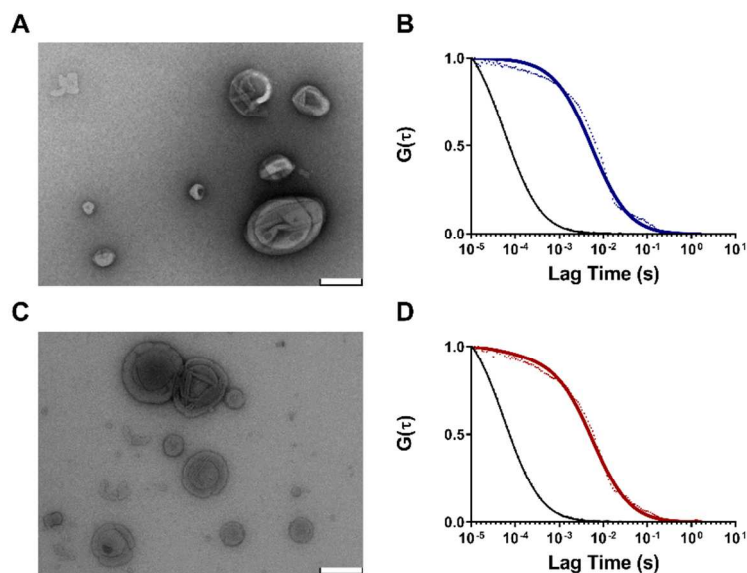
318 **_Figure 1._** _Formation of UOX-CNCs and HRP-CNCs._ **_A:_** _TEM micrograph of UOX-CNCs (scale bar: 200 nm)._ **_B_**_: normalized_

319 _FCS autocorrelation curve of the dye labeled UOX-CNCs (dots: normalized raw data; solid line: fitted data, black line: free_

320 _BODIPY 630/650)._ **_C_**_: TEM micrograph of HRP-CNCs (scale bar: 200 nm)._ **_D_**_: normalized FCS autocorrelation curve of the_

321 _dye-labeled HRP-CNCs (dots: normalized raw data; solid line: fitted data, black line: free BODIPY)._

322

323 _Overall enzymatic efficiency of CNCs_

324 Having determined the amounts of encapsulated enzymes, we used the same concentrations in

325 bulk to evaluate the efficiency of the cascade reaction. The cascade reaction takes place when the

326 enzymes are free or encapsulated in separate nanocompartments equipped with OmpF (Figure

327 2A). The reaction cannot proceed when the membrane of the nanocompartments is not equipped

328 with OmpF, to allow molecular passage through (Figure 2B), or when one of the enzymes or

329 substrates is removed from the cascade (Figure 2C).

Figure 2. *Cascade reaction with different setups. **A**: Enzyme kinetics when both enzymes are free (red), only HRP is free (light green), only UOX is free (dark green) and both UOX and HRP are encapsulated inside polymersomes (blue). **B**: Cascade with permeabilized CNCs (blue), unpermeabilized UOX-loaded polymersomes (olive), unpermeabilized HRP-loaded polymersomes (black). **C**: Cascade reaction with both CNCs and the corresponding substrates (blue), and in the absence of one of the reaction*

As expected, the cascade reaction between separate nanocompartments is significantly slower than that of the free enzymes. Going a step further, we were interested in establishing the effect of the molecular diffusion through OmpF of substrates and products, examining the probability that the product of the first reaction penetrates in a second CNC containing the HRP and studying the effect of the distance between different CNCs on each step of the reaction and on its overall efficiency. The conversion of AR to resorufin (AR conversion) was used as a comparison standard, because it represents the last step of the cascade reaction and therefore accounts for whether the whole cascade reaction takes place. First, we studied the influence of molecular diffusion through OmpF as a key factor, which might limit the *in situ* enzymatic reaction inside CNCs. Having one of the enzymes free in solution and the second one encapsulated in the CNCs, AR conversion decreased compared with that of free enzymes. When HRP was surrounding UOX-CNCs, a slight decrease in AR conversion to 92% was observed, while when UOX was free around the HRP-CNCs, a significant decrease in AR conversion to 13% was obtained (Figure 3). When both enzymes were encapsulated within the CNCs working in tandem, AR conversion decreased significantly to 3% after 15 minutes. As H_2O_2 is known to rapidly diffuse through OmpF and it passes through the same barriers (membrane and inter-vesicle space) regardless of which enzyme is inside the CNCs, its effect is only minor and is due to its probability to interact with HRP. When only UOX is inside the CNCs, the slight decrease in AR conversion is due to an inhomogeneous distribution of UOX-CNCs, which are the only source of H_2O_2. When HRP is inside the CNCs, the greater decrease in AR conversion is related to the slow diffusion of AR through the OmpF pores, which is also the bottleneck for the cascade

359   reaction between CNCs in tandem. Another factor that contributes to the significant decrease in

360   the reaction efficiency when CNCs are in tandem is the inhomogeneous CNC distribution which

361   reduces the probability that the substrates of the second reaction reach the HRP-CNCs. Besides,

362   the necessity of H_2O_2 transfer from UOX-CNCs to HRP-CNCs is proven by introducing free

363   catalase to the reaction mixture, as a competing enzyme that converts H_2O_2 to water and oxygen

364   (without Amplex Red as co-factor): when added, catalase strongly hinders the reaction mediated

365   by HRP (Figure S5A).

366
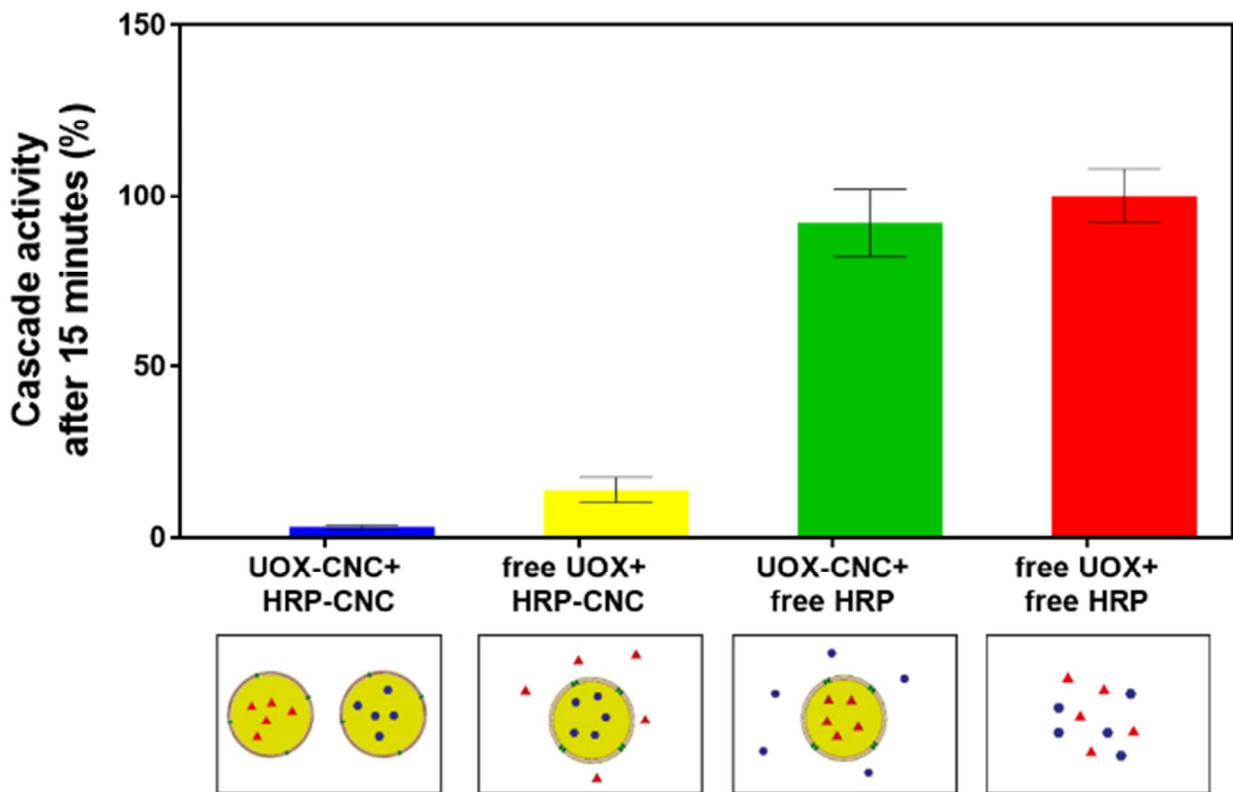
Figure 3. Conversion of AR to resorufin by a cascade enzymatic reaction when: both enzymes are encapsulated (blue), and only

HRP is encapsulated (HRP-CNCs) and UOX is free (yellow), only UOX is encapsulated (UOX-CNCs) and HRP is free (green),

both enzymes are free (red). Error bars are given as mean ± SD (n = 3).

370

371   *Kinetic analysis of CNCs*

372   It is already known that encapsulation in polymersomes affects the kinetic parameters of

373   enzymes, by increasing their affinity for the substrates or decreasing the velocity, because they

374   are in a different environment than in solution.[30] To characterize the behavior of CNCs, we first

375   compared the kinetic parameters of CNCs when isolated and then when acting in tandem by

376   using the Michaelis-Menten model (Table 1 and 2, Figure S6). Both steps of the cascade reaction

377   can be modeled in a first approximation by using Michaelis-Menten kinetics because in the first

378   reaction (UOX-CNCs) uric acid is added in excess, and for the second step both substrates are in

379   excess in the surroundings of the HRP-CNCs (AR added in excess in the medium, and H_2O_2

380   generated by UOX-CNCs with V_{max} of 1.47×10^{-3} μM/min, which is one order of magnitude

381   higher than V_{max} of HRP, as presented in Table 1 and 2).

382   K_M, the Michaelis-Menten constant, defines the affinity of the enzyme for the substrate, and the

383   apparent V_{max} represents the maximal velocity at which the enzyme operates once it is saturated

384   by the substrate. As both K_M and V_{max} are intrinsic characteristics of the enzymes in specific

385   conditions, it is expected that these parameters are not affected by the enzyme encapsulation (if

386   the substrate/products diffusion is not changing due to possible barriers). However, we observe a

387   completely different situation: both K_M and V_{max} are affected by enzyme encapsulation (Table 1

388   and 2).

389   The apparent K_M of both enzymes is lowered once confined in the nanocompartment, 4-times for

390   UOX-CNC and 1.5 times for HRP-CNC, which is in agreement with a previous publication

391   where encapsulated enzymes tend to exhibit a lowering in K_M.[34] However, this is not surprising

392   as the hollow cavity of a polymersome offers a more confined space, increasing the probability

393   of the substrate to access the catalytic center of the enzyme.[30] In addition, there is a decrease in

394   V_{max} and k_{cat} values. The decrease of both V_{max} and k_{cat} is significant in the case when UOX is

395   encapsulated in the CNCs (both for free HRP and for HRP-CNCs) (Table 1). On the contrary,

396   when HRP is encapsulated (free UOX and UOX-CNCs), the decrease in V_{max} and k_{cat} values is

397   noticeably smaller (Table 2). We assume the change in k_{cat} values is associated with a slower

398   influx of the substrates to the enzyme's active site, a slower efflux of the products or a

399   combination thereof when the enzymes are inside the CNCs due to various barriers associated

400   with the polymersomes architecture. Similarly, k_{cat}/K_M values decrease when the enzymes are

401   inside the CNCs. While the substrate can easily encounter the enzyme once inside the

402   compartment, the permeation through the membrane that is mediated by OmpF pores effectively

403   hinders the total activity of the cascade. The effect of diffusion to the enzyme is a well-known

404   parameter affecting and altering enzyme kinetics, as it can become the actual limiting factor in

405   their efficiency.[35-36]

Table 1. *Apparent kinetic parameters for UOX: Michaelis-Menten constant (K_M), maximal enzyme velocity (V_{max}), turnover rate (k_{cat}) and catalytic efficiency (k_{cat}/K_M).*

	Free UOX	Free UOX in cascade	UOX-CNC	UOX-CNC in cascade
K_M (µM)	3.70×10^2	3.68×10^2	8.32×10^1	9.09×10^1
V_{max} (µM/min)	2.47×10^{-1}	2.77×10^{-1}	1.22×10^{-4}	1.47×10^{-3}
k_{cat} (1/s)	2.72	2.55	1.34×10^{-3}	2.00×10^{-3}
k_{cat}/K_M (1/(µM s))	7.30×10^{-3}	7.52×10^{-3}	1.60×10^{-5}	2.20×10^{-5}

406

Table 2. *Apparent kinetic parameters for UOX: Michaelis-Menten constant (K_M), maximal enzyme velocity (V_{max}),*

turnover rate (k_{cat}) and catalytic efficiency (k_{cat}/K_M).

	Free HRP	**Free HRP in cascade**	**HRP-CNC**	**HRP-CNC in cascade**
K_M (μM)	$3.50×10$	$3.0×10$	$2.22×10$	$1.92×10$
V_{max} (μM/min)	$7.82×10^{-4}$	$8.19×10^{-4}$	$4.21×10^{-5}$	$1.32×10^{-4}$
k_{cat} (1/s)	$1.14×10^{-2}$	$1.12×10^{-2}$	$1.94×10^{-3}$	$6.19×10^{-3}$
k_{cat}/K_M (1/M/s)	$4.10×10^{-4}$	$4×10^{-4}$	$2.80×10^{-4}$	$3.22×10^{-4}$

407

408   We exclude that the decrease in enzyme activity inside the CNCs is due to the confinement of

409   enzymes: encapsulated UOX (molecular radius 4.27 nm[37]) and HRP (molecular radius 2.98

410   nm[38]) move free in a 1000-fold and 12000-fold greater volume inside the polymersome than their

411   intrinsic volume, respectively. We calculated the inner volume of polymersomes as the volume

412   of a sphere with a radius R = R_h – d, where *d* is the polymersome membrane thickness of 10.7

413   nm (previously determined for PMOXA$_6$-PDMS$_{44}$-PMOXA$_6$ compartments[39]).

414   *Role of compartmentalization on CNC activity*

415   In a similar manner as is the case for liposomes, the polymeric membrane of nanocompartments

416   is expected to offer protection of the encapsulated payload from external agents that would

417   degrade it, as for example proteolytic attack.[40] We wanted to establish the protective role of the

418　nanocompartments in the presence of physical factors such as high temperatures and different pH

419　values as well as degrading agents (GdnHCl and Proteinase K). We quantified the "activity

420　retention" as the ratio between the production of resorufin under standard conditions (RT, pH 7)

421　and in the presence of degrading conditions. Wild-type OmpF is known to be stable at relatively

422　extreme pH,[41-43] resistant to proteolysis,[44] chaotropic agents and temperatures up to 75 °C.[43]

423　Therefore, the porin is neither affected by the mild conditions of the rehydration method used to

424　generate the catalytic compartments, nor by the presence of a more complex environment or

425　degrading agents, because it is also protected inside the compartments membrane.

426　While below 37°C both encapsulated and free enzymes preserve their activity, for higher

427　temperatures, a decrease in activity is observed, but to a significantly higher degree for the free

428　enzymes (Figure 4A, Figure S5D and S7). The ability of the polymeric membrane to protect the

429　encapsulated payload from the effect of higher temperatures,[45-46] which denatures the enzymes,

430　is essential for translational applications. The effect of pH was less straight forward, as these two

431　enzymes have a different pH optima: basic for UOX and acidic for HRP.[47-48] While at pH 3 there

432　is no apparent gain in activity from the enzyme encapsulation, at pH 9 the CNCs are significantly

433　more active than the free enzymes acting in tandem (Figure 4B). The enzyme activity is further

434　affected upon encapsulation due to a complex scenario: i) the interplay between the lower

435　stability of HRP at higher pH values[49] and the basic pH optimum of UOX, ii) the stabilization of

436　HRP –known to interact with hydrophobic substrates[50]– once inside the compartment, and iii) an

437　increase in enzyme accessibility for the substrates due to the confined reaction space.[30] Therefore

438　the effect of the pH on activity is less evident when the enzymes are free in solution and no

439　confinement effects are present. However, we chose a neutral pH to evaluate the CNCs in

440　tandem to be closer to physiological conditions, at which both enzymes are still active (Figure

441   S5B), and where both the free enzymes and encapsulated ones have similar activity retention

442   values.

443   The addition of an enzyme denaturing chemical agent, such as GdnHCl, decreased the enzyme

444   activity, which is significantly more pronounced when the enzymes are free. This clearly

445   indicates the protective role of compartmentalization (Figure 4C). The decrease in activity

446   retention values in the case of CNCs in tandem is mainly due to the diffusion of GdnHCl (95 Da)

447   through OmpF, which has a weight cut-off of 650 Da.[51] Even though in a previous report

448   GdnHCl diffused through the polymersome membrane,[52] this is not observed here as shown by

449   the highly retained activity. The permeability of PMOXA-PDMS-PMOXA membranes varies

450   depending on the molecular factors, such as the thickness of the membrane, the polydispersity of

451   the copolymer chains or the conditions in which they are formed. In addition to the small number

452   of inserted OmpF that are enough to allow *in situ* enzymatic reaction, the innate resistance

453   towards denaturation of UOX [53-54] and the possible stabilization of HRP due to interactions with

454   the membrane are responsible for maintaining enzymes' activity in the case of our CNCs, even in

455   presence of GdnHCl.

456   To mimic a proteolytic attack, we added Proteinase K both to free enzymes and the CNCs for 2

457   hours. While a significant decrease in activity retention was observed for the free enzymes (18 ±

458   1%), in the case of CNCs the decrease was considerably smaller (83 ± 3%), additionally showing

459   that a small fraction of enzyme molecules was adsorbed at the outer interface of the

460   polymersome[33] (Figure 4D). We considered the overall activity of the CNCs as a whole;

461   however, by adding free enzymes to empty vesicles and then purifying them, it was possible to

462   detect a certain amount of activity due to unspecific binding in the cascade for HRP, estimated to

463   be around 3% of the total (Figure S5C and Table S1). The auto-oxidation of AR was also taken

464   into account, and subtracted in all blanks.

465
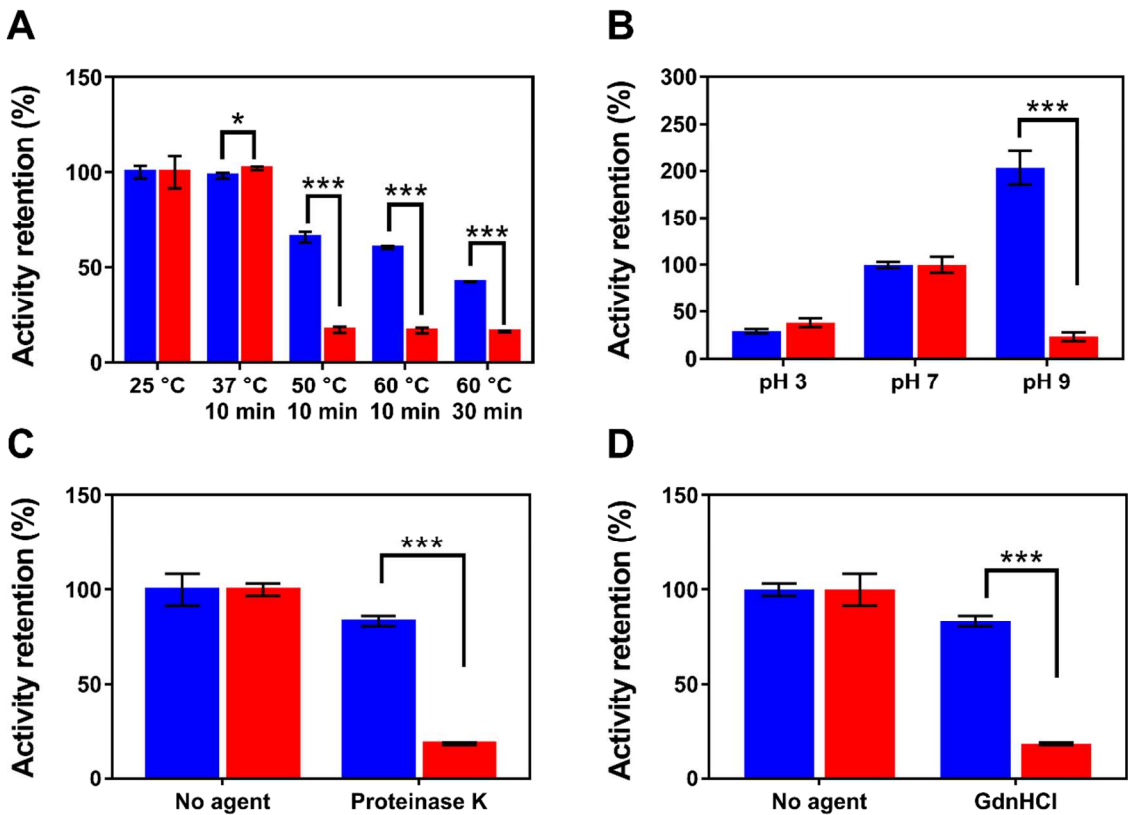
466   **Figure 4**. *Stability of catalytic nanocompartments and free enzymes (activity normalized against CNCs (blue) or enzymes (red) at*

467   *RT, neutral pH, no agents).* **A**: *protection from heat.* **B**: *protection from extreme pH.* **C**: *protection from denaturing agent*

468   *GdnHCl.* **D**: *protection from proteolysis. Error bars are given as mean ± SD (multiple t - test, * p < 0.05, ** p < 0.01, *** p <*

469   *0.001, n = 3).*

470

471   *The effect of distance on the efficiency of the CNCs in tandem*

472   The passage through barriers and diffusion between compartments represents an essential point

473   in bio-communication because products have, in some cases, to travel to different cellular

474   compartments or take part in inter-cellular communication. Most organelle-to-organelle

475 communications in the cell happen via close association below 50 nm[55] and the average synaptic

476 cleft is around 20 nm,[56] whereas it is estimated that a single cell can effectively communicate

477 between 5 and 10 μm in autocrine signaling and up to 250 μm in paracrine signaling.[57-58] In such

478 cases of communication between organelles or cells, there is no longer a homogeneous

479 distribution of enzymes or receptors but local high concentrations and otherwise empty or low

480 density interstices. We used our CNCs in tandem to mimic communication between bio-

481 assemblies and see the effect of distance on the overall cascade reaction efficiency. We assumed

482 a cubic volume for the compartments, so that the mean inter-compartment distance is calculated,

483 based on the polymersome density obtained by FCS.

484 The AR conversion values in the case of CNCs in tandem remains almost constant (with some

485 values higher than 100% as values fluctuate around the mean obtained at 0.8 μm, set as

486 reference) until the mean distance between CNCs is 1.3 μm, then the values decrease

487 significantly. This suggests that the diffusion of molecules through the OmpF pores represents

488 the dominant factor for distances lower than approximately 1.30 μm. Interestingly, the ratio

489 between the mean inter-compartment distance and their diameter is about 10, which has the same

490 order of magnitude as the ratio between a mean cell-cell communication distance for cells with a

491 1 μm diameter, such as bacteria.[59] For distances between CNCs higher than 1.3 μm, the cascade

492 reaction is rapidly hindered due to a decrease in the probability that H_2O_2 encounters a HRP-

493 CNC (Figure 5). These distances are consistent with distances typical for autocrine signaling.

494 Therefore our findings, based on tandem CNCs in a simplified medium, represents a first

495 necessary step for better understanding cell communication.

496
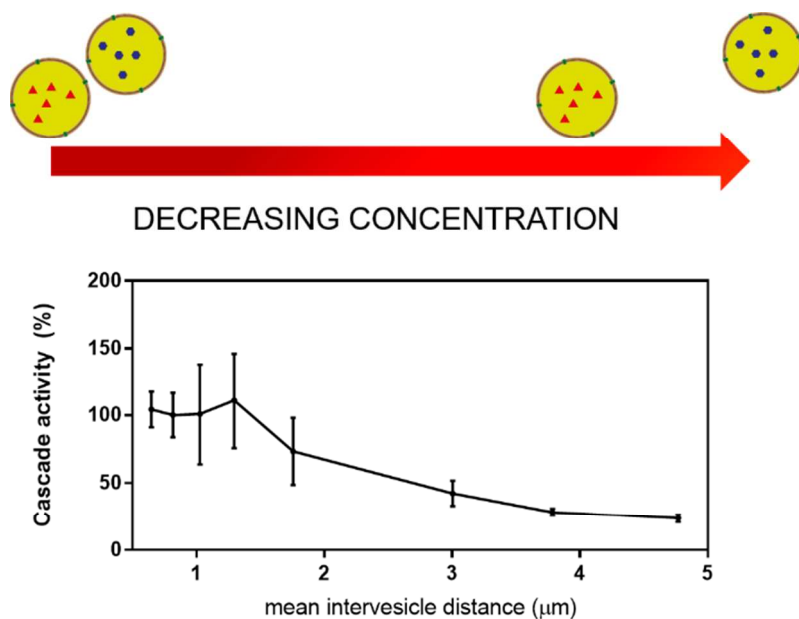
Figure 5. AR conversion by cascade reaction inside CNCs in tandem at different mean inter-vesicle distances. Error bars are

*given as mean ± SD (n = 3).*

CNCs in tandem in biologic conditions

We then evaluated the functionality of the CNCs in biological conditions, both in biofluids and

upon incubation with cells, as more apropriate to advance translational applications. First, we

used human blood serum where uric acid was dissolved to reach levels similar to those

considered typical for hyperucemia (>6.8 mg dL^{-1} in men[60]). A simple model, defined as

$$\frac{\frac{\Delta Abs290_{with\ enzyme}}{min}}{\frac{\Delta Abs290_{no\ enzyme}}{min}}$$ for the dilutions of HRP-CNCs, gives the relative efficiency of the cascade

reaction, which we called Relative Urate Degradation (R.U.D.) (Figure 6A). Interestingly, in

such a complex medium, CNCs facilitate the clearance of uric acid at a comparable rate to the

free enzyme. The addition of HRP removes H_2O_2, pulling the first reaction forward according to

Le Chatelier's principle. In addition, we observed no aggregation of polymersomes in serum, in

agreement with reported results on similar polymers.[61] Note that only in PBS the free enzymes

510   are better in terms of the cascade efficiency than when encapsulated inside polymersomes.

511   However, in serum, they perform similarly, which emphasizes the role of the compartments in

512   protecting the encapsulated enzymes in these conditions (37 °C, 6 hours), and support our

513   approach for further cell assessment. Further studies, beyond the scope of the present one, are

514   necessary to understand the bio-molecular factors affecting the efficiency of the overall cascade

515   reaction between CNCs in human serum.

516   Second, we determined the ability of the CNCs to metabolize uric acid and degrade H_2O_2 upon

517   incubation with cells, as an essential step towards medical applications. First, we evaluated the

518   cytotoxicity of CNCs when incubated with HEK293T cells overnight at different concentrations

519   of the CNCs (measured in polymer concentration) by MTS assay. CNCs have no cytotoxic effect

520   towards the cells, even at the highest polymer concentration (0.19 µg mL^{-1}) (Figure 6B). Next,

521   CNCs were incubated with HEK293T epithelial cells for 24 h in the presence of increasing

522   amounts of uric acid (250 and 350 µM): at physiological concentration and at the lower end of

523   hyperuricemia values. CNCs, known to be eventually internalized by cells,[7] were added together

524   with uric acid because it accumulates extracellularly to toxic levels: in this manner CNCs

525   directly protect cells by degrading uric acid. Cell viability decreased to around 60% in the

526   presence of 250 µM uric acid. By addition of either free enzymes or the CNCs, the cell viability

527   was unaffected by the presence of uric acid. Increasing the amount of uric acid to 350 µM

528   reduces the viability of the cells to 2%, while the cascade reaction of the free enzymes and of the

529   CNCs in tandem induce a protective effect against uric acid. In addition, due to the combination

530   of enzymes, H_2O_2 is also degraded as a result of the succesful cascade reaction process (Figure

531   6C and D).
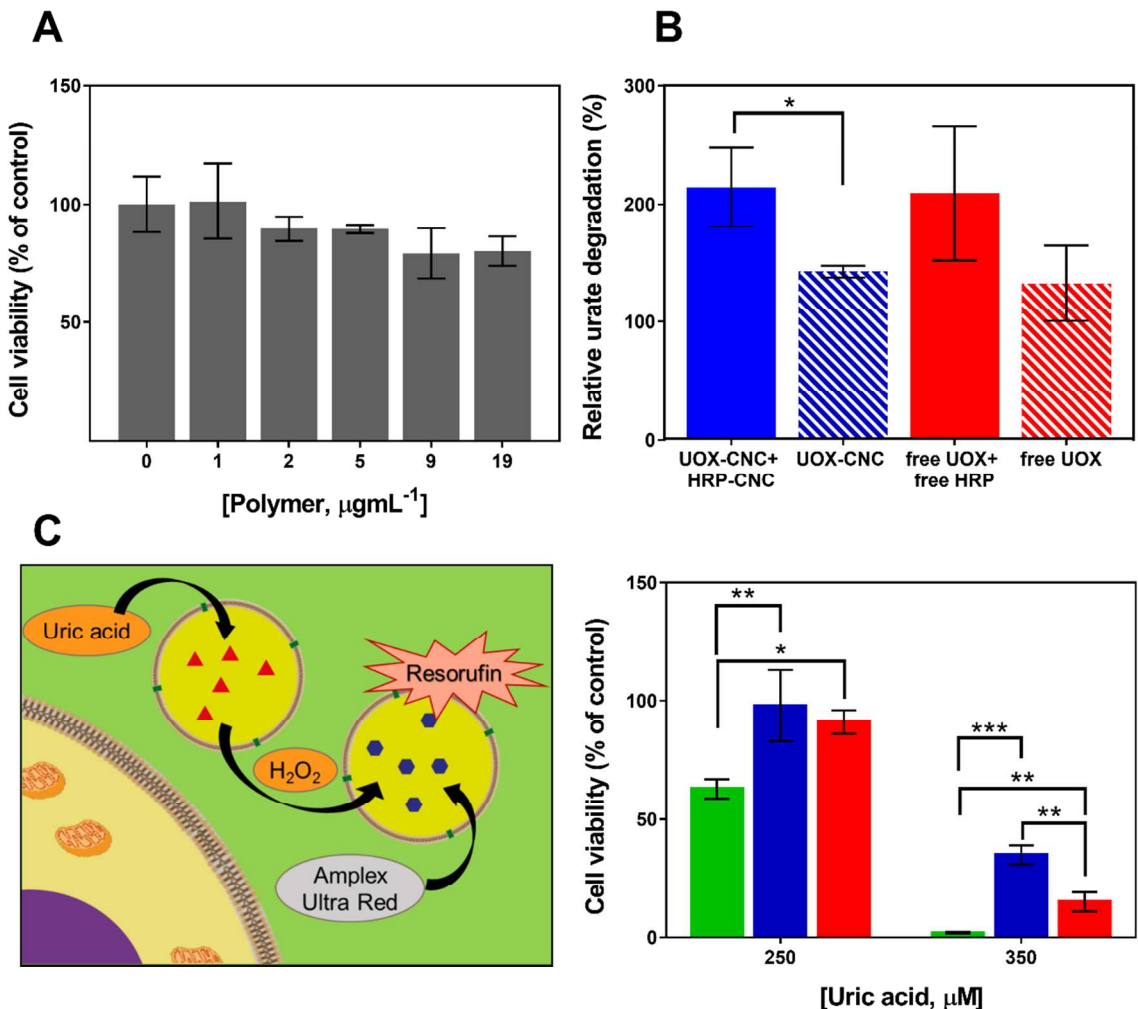
Figure 6. *Activity of CNCs and free enzymes in blood serum and their interaction with cells. **A**: clearance of urate with both CNCs (solid blue), UOX-CNC only (striped blue, no HRP-CNC), both free enzymes (solid red) and UOX only (striped red, no HRP-CNC) **B**: cell viability of HEK293T cells incubated with CNCs at different concentrations (expressed as polymer concentration). **C:** scheme of the CNC-cell interaction and detoxifying activity of the UOX-HRP cascade on cells only (green), cells with free enzymes (blue) and cells with CNCs (red). Error bars are given as mean ± SD (multiple t - test, * p < 0.05, ** p < 0.01, *** p < 0.001, n = 3).*

Conclusions

We designed two spatially segregated catalytic nanocompartments to support a cascade reaction between them, mimicking sequential reactions between biosystems. By an elegant selection of

542 the enzyme combination, we applied these catalytic nanocompartments in tandem to decrease

543 uric acid and H_2O_2, both involved in various pathologic conditions ranging from gout to

544 oxidative stress. A thorough analysis of the factors affecting the overall efficiency of the cascade

545 reaction between CNCs indicated the protective role of the compartments, which provide a shield

546 for the encapsulated enzymes, especially important in biological fluids and cellular environment.

547 For the first time, a kinetic evaluation of a cascade reaction between segregated reaction spaces

548 at the nanoscale has been achieved. We elucidated the limiting factors for the overall reaction: i)

549 the diffusion through the membrane pores inserted into the walls of the compartments and ii) the

550 probability of the products from the first reaction to encounter CNCs containing the second

551 enzyme and reach the encapsulated enzyme molecules. A balance is necessary between the

552 protective role of the nanocompartments and the factors that decrease the efficiency of the

553 cascade reaction for translational applications. This cascade reaction in separate compartments

554 has been successfully performed in serum and then used to decrease both uric acid and the

555 derived H_2O_2 from the cellular milieu as a first step towards medical applications. Our study is

556 the first one that proves that a two-compartment cascade reaction acts in cellular conditions, thus

557 contributing to the understanding of the design of complex catalytic compartments to cope with

558 biological requirements.

559

560 **Supporting Information**

561 Supporting information: additional physical characterization, enzymatic assays in various

562 conditions, Michaelis-Menten curves. (PDF)

563 **Corresponding Author**

564   Prof. Dr. Cornelia G. Palivan, Department of Chemistry, Physical Chemistry, Mattenstrasse 24a,

565   CH-4058 Basel

566   cornelia.Palivan@unibas.ch

Author Contributions

568   A.B contributed to the CNCs production and characterization, I.C contributed to the *in vitro*

569   assays, J.L. contributed to experiment design and enzymatic assays, and C.G.P contributed to the

570   concept of CNCs in tandem. The manuscript was written through contributions of all authors.

571   All authors have given approval to the final version of the manuscript.

REFERENCES

582   1.   Kuchler, A.; Yoshimoto, M.; Luginbuhl, S.; Mavelli, F.; Walde, P., Enzymatic reactions
583   in confined environments. *Nat Nanotechnol* **2016,** *11* (5), 409-20.
584   2.   Agapakis, C. M.; Boyle, P. M.; Silver, P. A., Natural strategies for the spatial
585   optimization of metabolism in synthetic biology. *Nat Chem Biol* **2012,** *8* (6), 527-35.
586   3.   Hosta-Rigau, L.; York-Duran, M. J.; Zhang, Y.; Goldie, K. N.; Stadler, B., Confined
587   multiple enzymatic (cascade) reactions within poly(dopamine)-based capsosomes. *ACS Appl
588   Mater Interfaces* **2014,** *6* (15), 12771-9.

589   4.   Sakr, O. S.; Borchard, G., Encapsulation of Enzymes in Layer-by-Layer (LbL)
590   Structures: Latest Advances and Applications. *Biomacromolecules* **2013,** *14* (7), 2117-2135.
591   5.   Palivan, C. G.; Fischer-Onaca, O.; Delcea, M.; Itel, F.; Meier, W., Protein-polymer
592   nanoreactors for medical applications. *Chem Soc Rev* **2012,** *41* (7), 2800-23.
593   6.   Schoonen, L.; van Hest, J. C., Compartmentalization Approaches in Soft Matter Science:
594   From Nanoreactor Development to Organelle Mimics. *Adv Mater* **2016,** *28* (6), 1109-28.
595   7.   Tanner, P.; Onaca, O.; Balasubramanian, V.; Meier, W.; Palivan, C. G., Enzymatic
596   cascade reactions inside polymeric nanocontainers: a means to combat oxidative stress.
597   *Chemistry* **2011,** *17* (16), 4552-60.
598   8.   Blackman, L. D.; Varlas, S.; Arno, M. C.; Fayter, A.; Gibson, M. I.; O'Reilly, R. K.,
599   Permeable Protein-Loaded Polymersome Cascade Nanoreactors by Polymerization-Induced Self-
600   Assembly. *ACS Macro Lett* **2017,** *6* (11), 1263-1267.
601   9.   Peters, R. J.; Marguet, M.; Marais, S.; Fraaije, M. W.; van Hest, J. C.; Lecommandoux,
602   S., Cascade reactions in multicompartmentalized polymersomes. *Angew Chem Int Ed Engl* **2014,**
603   *53* (1), 146-50.
604   10.   Grafe, D.; Gaitzsch, J.; Appelhans, D.; Voit, B., Cross-linked polymersomes as
605   nanoreactors for controlled and stabilized single and cascade enzymatic reactions. *Nanoscale*
606   **2014,** *6* (18), 10752-61.
607   11.   Taek, K. K.; M., C. J. J. L.; M., N. R. J.; M., v. H. J. C., A Polymersome Nanoreactor
608   with Controllable Permeability Induced by Stimuli-Responsive Block Copolymers. *Advanced*
609   *Materials* **2009,** *21* (27), 2787-2791.
610   12.   Schmitt, C.; Lippert, A. H.; Bonakdar, N.; Sandoghdar, V.; Voll, L. M.,
611   Compartmentalization and Transport in Synthetic Vesicles. *Front Bioeng Biotechnol* **2016,** *4*, 19.
612   13.   Lomora, M.; Garni, M.; Itel, F.; Tanner, P.; Spulber, M.; Palivan, C. G., Polymersomes
613   with engineered ion selective permeability as stimuli-responsive nanocompartments with
614   preserved architecture. *Biomaterials* **2015,** *53* (0), 406-414.
615   14.   van Oers, M. C.; Rutjes, F. P.; van Hest, J. C., Cascade reactions in nanoreactors. *Curr*
616   *Opin Biotechnol* **2014,** *28*, 10-6.
617   15.   Bolinger, P. Y.; Stamou, D.; Vogel, H., An integrated self-assembled nanofluidic system
618   for controlled biological chemistries. *Angew Chem Int Ed Engl* **2008,** *47* (30), 5544-9.
619   16.   Brasch, M.; Putri, R. M.; de Ruiter, M. V.; Luque, D.; Koay, M. S.; Caston, J. R.;
620   Cornelissen, J. J., Assembling Enzymatic Cascade Pathways inside Virus-Based Nanocages
621   Using Dual-Tasking Nucleic Acid Tags. *J Am Chem Soc* **2017,** *139* (4), 1512-1519.
622   17.   Marguet, M.; Bonduelle, C.; Lecommandoux, S., Multicompartmentalized polymeric
623   systems: towards biomimetic cellular structure and function. *Chem Soc Rev* **2013,** *42* (2), 512-29.
624   18.   Godoy-Gallardo, M.; Labay, C.; Jansman, M. M. T.; Ek, P. K.; Hosta-Rigau, L.,
625   Intracellular Microreactors as Artificial Organelles to Conduct Multiple Enzymatic Reactions
626   Simultaneously. *Advanced Healthcare Materials* **2016,** *6* (4), 1601190.
627   19.   Kuiper, S. M.; Nallani, M.; Vriezema, D. M.; Cornelissen, J. J.; van Hest, J. C.; Nolte, R.
628   J.; Rowan, A. E., Enzymes containing porous polymersomes as nano reaction vessels for cascade
629   reactions. *Org Biomol Chem* **2008,** *6* (23), 4315-8.
630   20.   Liu, X.; Formanek, P.; Voit, B.; Appelhans, D., Functional Cellular Mimics for the
631   Spatiotemporal Control of Multiple Enzymatic Cascade Reactions. *Angewandte Chemie*
632   *International Edition* **2017,** *56* (51), 16233-16238.

633   21.   Wang, Z.; van Oers, M. C. M.; Rutjes, F. P. J. T.; van Hest, J. C. M., Polymersome
634   Colloidosomes for Enzyme Catalysis in a Biphasic System. *Angewandte Chemie* **2012,** *124* (43),
635   10904-10908.
636   22.   Wertheimer, A.; Morlock, R.; Becker, M. A., A revised estimate of the burden of illness
637   of gout. *Current therapeutic research, clinical and experimental* **2013,** *75*, 1-4.
638   23.   Lörcher, S.; Meier, W., Cosolvent fractionation of PMOXA-b-PDMS-b-PMOXA: Bulk
639   separation of triblocks from multiblocks. *European Polymer Journal* **2017,** *88*, 575-585.
640   24.   Nardin, C.; Thoeni, S.; Widmer, J.; Winterhalter, M.; Meier, W., Nanoreactors based on
641   (polymerized) ABA-triblock copolymer vesicles. *Chemical Communications* **2000,** (15), 1433-
642   1434.
643   25.   Azmi, N. E.; Ramli, N. I.; Abdullah, J.; Abdul Hamid, M. A.; Sidek, H.; Abd Rahman,
644   S.; Ariffin, N.; Yusof, N. A., A simple and sensitive fluorescence based biosensor for the
645   determination of uric acid using H2O2-sensitive quantum dots/dual enzymes. *Biosens*
646   *Bioelectron* **2015,** *67*, 129-33.
647   26.   Dai, M.; Huang, T.; Chao, L.; Xie, Q.; Tan, Y.; Chen, C.; Meng, W., Horseradish
648   peroxidase-catalyzed polymerization of L-DOPA for mono-/bi-enzyme immobilization and
649   amperometric biosensing of H2O2 and uric acid. *Talanta* **2016,** *149*, 117-123.
650   27.   Miland, E.; Miranda Ordieres, A. J.; Tunon Blanco, P.; Smyth, M. R.; Fagain, C. O.,
651   Poly(o-aminophenol)-modified bienzyme carbon paste electrode for the detection of uric acid.
652   *Talanta* **1996,** *43* (5), 785-96.
653   28.   Einfalt, T.; Goers, R.; Dinu, I. A.; Najer, A.; Spulber, M.; Onaca-Fischer, O.; Palivan, C.
654   G., Stimuli-Triggered Activity of Nanoreactors by Biomimetic Engineering Polymer
655   Membranes. *Nano Lett* **2015,** *15* (11), 7596-603.
656   29.   JW. Krieger; Langowski, J. *QuickFit 3.0: A data evaluation application for biophysics*,
657   http://www.dkfz.de/Macromol/quickfit/, 2015.
658   30.   Baumann, P.; Spulber, M.; Fischer, O.; Car, A.; Meier, W., Investigation of Horseradish
659   Peroxidase Kinetics in an "Organelle-Like" Environment. *Small* **2017,** *13* (17).
660   31.   Stauch, O.; Schubert, R., Structure of Artificial Cytoskeleton Containing Liposomes in
661   Aqueous Solution Studied by Static and Dynamic Light Scattering. *Biomacromolecules* **2002**.
662   32.   Habel, J.; Ogbonna, A.; Larsen, N.; Cherre, S.; Kynde, S.; Midtgaard, S. R.; Kinoshita,
663   K.; Krabbe, S.; Jensen, G. V.; Hansen, J. S.; Almdal, K.; Helix-Nielsen, C., Selecting analytical
664   tools for characterization of polymersomes in aqueous solution. *RSC Advances* **2015,** *5* (97),
665   79924-79946.
666   33.   Edlinger, C.; Einfalt, T.; Spulber, M.; Car, A.; Meier, W.; Palivan, C. G., Biomimetic
667   Strategy To Reversibly Trigger Functionality of Catalytic Nanocompartments by the Insertion of
668   pH-Responsive Biovalves. *Nano Lett* **2017,** *17* (9), 5790-5798.
669   34.   Chen, Q.; Schönherr, H.; Vancso, G. J., Block-Copolymer Vesicles as Nanoreactors for
670   Enzymatic Reactions. *Small* **2009,** *5* (12), 1436-1445.
671   35.   Bar-Even, A.; Noor, E.; Savir, Y.; Liebermeister, W.; Davidi, D.; Tawfik, D. S.; Milo, R.,
672   The moderately efficient enzyme: evolutionary and physicochemical trends shaping enzyme
673   parameters. *Biochemistry* **2011,** *50* (21), 4402-10.
674   36.   Garcia-Viloca, M.; Gao, J.; Karplus, M.; Truhlar, D. G., How enzymes work: analysis by
675   modern rate theory and computer simulations. *Science* **2004,** *303* (5655), 186-95.
676   37.   Caliceti, P.; Schiavon, O.; Veronese, F. M., Biopharmaceutical properties of uricase
677   conjugated to neutral and amphiphilic polymers. *Bioconjug Chem* **1999,** *10* (4), 638-46.

678   38.   Rennke, H. G.; Patel, Y.; Venkatachalam, M. A., Glomerular filtration of proteins:
679   clearance of anionic, neutral, and cationic horseradish peroxidase in the rat. *Kidney Int* **1978,** *13*
680   (4), 278-88.
681   39.   Itel, F.; Chami, M.; Najer, A.; Lörcher, S.; Wu, D.; Dinu, I. A.; Meier, W., Molecular
682   Organization and Dynamics in Polymersome Membranes: A Lateral Diffusion Study.
683   *Macromolecules* **2014,** *47* (21), 7588-7596.
684   40.   Cao, X.; Chen, C.; Yu, H.; Wang, P., Horseradish peroxidase-encapsulated chitosan
685   nanoparticles for enzyme-prodrug cancer therapy. *Biotechnology letters* **2015,** *37* (1), 81-8.
686   41.   Ihle, S.; Onaca, O.; Rigler, P.; Hauer, B.; Rodríguez-Ropero, F.; Fioroni, M.;
687   Schwaneberg, U., Nanocompartments with a pH release system based on an engineered OmpF
688   channel protein. *Soft Matter* **2011,** *7* (2), 532-539.
689   42.   Nestorovich, E. M.; Rostovtseva, T. K.; Bezrukov, S. M., Residue Ionization and Ion
690   Transport through OmpF Channels. *Biophysical Journal* **2003,** *85* (6), 3718-3729.
691   43.   Phale, P. S.; Philippsen, A.; Kiefhaber, T.; Koebnik, R.; Phale, V. P.; Schirmer, T.;
692   Rosenbusch, J. P., Stability of trimeric OmpF porin: the contributions of the latching loop L2.
693   *Biochemistry* **1998,** *37* (45), 15663-70.
694   44.   Mukherjee, S.; Guptasarma, P., Direct proteolysis-based purification of an overexpressed
695   hyperthermophile protein from Escherichia coli lysate: a novel exploitation of the link between
696   structural stability and proteolytic resistance. *Protein Expression and Purification* **2005,** *40* (1),
697   71-76.
698   45.   Yan, M.; Ge, J.; Liu, Z.; Ouyang, P., Encapsulation of Single Enzyme in Nanogel with
699   Enhanced Biocatalytic Activity and Stability. *Journal of the American Chemical Society* **2006,**
700   *128* (34), 11008-11009.
701   46.   Cecchin, D.; Battaglia, G. In *Protein stabilisation by polymersome entrapment*, **2016**.
702   47.   Critchlow, J. E.; Dunford, H. B., Studies on Horseradish Peroxidase *The Journal of*
703   *Biological Chemistry* **1972**.
704   48.   Mahler, H. R. a.; Baum, H. M. c.; Hübscher, G., Enzymatic oxidation of urate. *Science*
705   **1956**.
706   49.   Moosavi-Movahedi, A. A.; Nazari, K.; Saboury, A. A., Thermodynamics of denaturation
707   of horseradish peroxidase with sodium n-dodecyl sulphate and n-dodecyl trimethylammonium
708   bromide. *Colloids and Surfaces B: Biointerfaces* **1997,** *9* (3), 123-130.
709   50.   Di Risio, S.; Yan, N., Adsorption and inactivation behavior of horseradish peroxidase on
710   cellulosic fiber surfaces. *J Colloid Interface Sci* **2009,** *338* (2), 410-419.
711   51.   Saint, N.; Lou, K. L.; Widmer, C.; Luckey, M.; Schirmer, T.; Rosenbusch, J. P.,
712   Structural and functional characterization of OmpF porin mutants selected for larger pore size. II.
713   Functional characterization. *J Biol Chem* **1996,** *271* (34), 20676-80.
714   52.   Rosenkranz, T.; Katranidis , A.; Atta, D.; Gregor , I.; Enderlein, J.; Grzelakowski, M.;
715   Rigler, P.; Meier, W.; Fitter, J., Observing Proteins as Single Molecules Encapsulated in Surface-
716   Tethered Polymeric Nanocontainers. *ChemBioChem* **2009,** *10* (4), 702-709.
717   53.   Pitts, O. M.; Priest, D. G.; Fish, W. W., Uricase. Subunit composition and resistance to
718   denaturants. *Biochemistry* **1974,** *13* (5), 888-92.
719   54.   Pace, C. N.; Hermans, J., The Stability of Globular Protein. *CRC Critical Reviews in*
720   *Biochemistry* **1975,** *3* (1), 1-43.
721   55.   Achleitner, G.; Gaigg, B.; Krasser, A.; Kainersdorfer, E.; Kohlwein, S. D.; Perktold, A.;
722   Zellnig, G.; Daum, G., Association between the endoplasmic reticulum and mitochondria of

723   yeast facilitates interorganelle transport of phospholipids through membrane contact. *Eur J*
724   *Biochem* **1999,** *264* (2), 545-53.
725   56.   Barberis, A.; Petrini, E. M.; Mozrzymas, J. W., Impact of synaptic neurotransmitter
726   concentration time course on the kinetics and pharmacological modulation of inhibitory synaptic
727   currents. *Front Cell Neurosci* **2011,** *5*, 6.
728   57.   Francis, K.; Palsson, B. O., Effective intercellular communication distances are
729   determined by the relative time constants for cyto/chemokine secretion and diffusion. *Proc Natl*
730   *Acad Sci U S A* **1997,** *94* (23), 12258-62.
731   58.   Shvartsman, S. Y.; Wiley, H. S.; Deen, W. M.; Lauffenburger, D. A., Spatial range of
732   autocrine signaling: modeling and computational analysis. *Biophys J* **2001,** *81* (4), 1854-67.
733   59.   Chien, A. C.; Hill, N. S.; Levin, P. A., Cell size control in bacteria. *Curr Biol* **2012,** *22*
734   (9), R340-9.
735   60.   Maiuolo, J.; Oppedisano, F.; Gratteri, S.; Muscoli, C.; Mollace, V., Regulation of uric
736   acid metabolism and excretion. *Int J Cardiol* **2016,** *213*, 8-14.
737   61.   Murdoch, C.; Reeves, K. J.; Hearnden, V.; Colley, H.; Massignani, M.; Canton, I.;
738   Madsen, J.; Blanazs, A.; Armes, S. P.; Lewis, A. L.; Macneil, S.; Brown, N. J.; Thornhill, M. H.;
739   Battaglia, G., Internalization and biodistribution of polymersomes into oral squamous cell
740   carcinoma cells in vitro and in vivo. *Nanomedicine* **2010,** *5* (7), 1025-36.

741